^{1}H Nuclear magnetic resonance investigation of cobalt(II) substituted carbonic anhydrase

Lucia Banci,* L. B. Dugad,‡ Gerd N. La Mar,‡ Kelly A. Keating,‡ Claudio Luchinat,§ and Roberta Pierattelli*
*Department of Chemistry, University of Florence, Florence, Italy; ‡Department of Chemistry, University of California, Davis, USA; and §Institute of Agricultural Chemistry, University of Bologna, Bologna, Italy

ABSTRACT The structure of ClO_4^- and NO_3^- adducts of cobalt(II) substituted bovine carbonic anhydrase have been investigated through 1D NOE and 2D ^{1}H nuclear magnetic resonance (NMR) spectroscopy. For the first time two-dimensional NMR techniques are applied to paramagnetic metalloproteins other than iron-containing proteins. Several active site signals have been assigned to specific protons on the grounds of their scalar and dipolar connectivities and T_1 values. The experimental dipolar shifts for the protons belonging to noncoordinated residues have allowed the identification of a plausible orientation of the magnetic susceptibility tensor around the cobalt ion as well as of the magnitude and the anisotropy of the principal susceptibility values. In turn, a few more signals have been tentatively assigned on the grounds of their predicted dipolar shifts.

The two inhibitor derivatives have a very similar orientation but a different magnitude of the χ tensor, and the protein structure around the active site is highly maintained.

The results encourage a more extensive use of two-dimensional techniques for obtaining selective structural information on the active site of metalloenzymes. With this information at hand, comparisons within homologous series of adducts with various inhibitors and/or of mutants of the same enzyme of known structure should be possible using limited sets of NMR data.

INTRODUCTION

The hyperfine shifts of paramagnetic metalloproteins contain unique and valuable information on two distinct aspects of the active site (1, 2). The through-bond or contact interaction provides information on oxidation/spin state of the metal ion and the nature of the metal-ligand bonding. The majority of ^{1}H nuclear magnetic resonance (NMR) studies have focused on the information content of the contact shifts. Dipolar shifts result from magnetic susceptibility anisotropy of the metal ion. The anisotropy arises from the presence of spin-orbit coupling and is commonly present, to various degrees, in all transition metal complexes. Thus, analysis of dipolar shifts is a general way to provide information on the orientation of the magnetic axes which define the magnetic susceptibility tensor with respect to structural elements of the bonding geometry. On the other hand, if the orientation of the magnetic susceptibility tensor is known, dipolar shifts can be used to find out the orientation of nonbonded active site residues with respect to these magnetic axes. Therefore, the dipolar shifts could, in principle, be interpreted in terms of detailed structure, either alone, or in conjunction with nuclear Overhauser, NOE, constraints conventionally used for diamagnetic systems (3).

To effectively utilize the dipolar shift for structural studies, the metal ion must possess significant magnetic anisotropy so as to produce a reasonably well-resolved ^{1}H NMR spectrum, and at the same time leave the resonances sufficiently narrow so that they can be assigned by modern NMR methodology. Two common metal ions frequently display these two favorable characteristics, low-spin iron(III) and high-spin cobalt(II), of which the former can be prepared for a wide variety of native hemoproteins. Recent advances in NMR methodology for paramagnetic complexes allow the required assignments that are crucial for the quantitative analysis of dipolar shifts. To date, the majority of the NMR studies have been performed on low-spin ferric systems such as cytocromes *c* and cyanometmyoglobin, where the magnetic axes have been determined quantitatively, the orientation of the axes interpreted in terms of bonding constraints, and the dipolar shifts of nonbonded residues analyzed in terms of detailed solution structure (4–6).

In addition, the nuclear relaxation enhancement due to the coupling of the magnetic nucleus with the unpaired electrons provides further valuable information on the coordination geometry of the metal ion and on the structural arrangement of the residues close to the metal center.

For nonbonded residues, the enhancement in T_1^{-1} again originates from dipolar coupling with the paramagnetic center and then depends on the reciprocal of the sixth power of the distance between the metal ion and the nucleus. This enhancement provides, therefore, direct structural information. At the same time, nuclear relaxation rate enhancement depends on the electron relaxation rates, which in turn are related to the oxidation/spin state and coordination geometry of the metal ion.

High-spin cobalt(II) does not occur naturally in metalloenzymes but is frequently used as a sensitive spectroscopic probe in a variety of zinc metalloproteins (7), the utility of the cobalt(II) based spectroscopic data is validated by the partial to total retention of activity of these enzymes (8). Native carbonic anhydrase, (CA) has a molecular weight of 30,000 and contains a tetrahedrally coordinated zinc(II) ion (9) (Fig. 1). Substitution by co-

Address correspondence to Dr. Luchinat.

0006-3495/92/08/530/14 $2.00

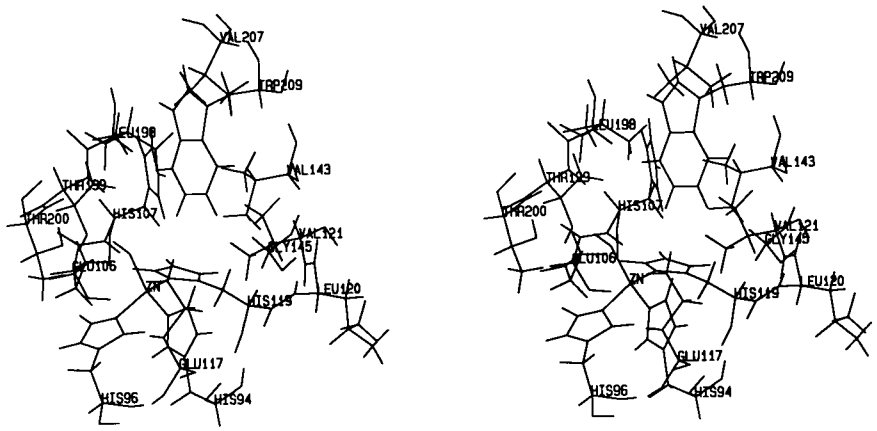

FIGURE 1 Stereoview of the coordination sphere of zinc(II) ion in HCA II[9] and of some active site residues discussed in the present paper.

balt(II) yields an active enzyme (10) but in this system high-spin cobalt(II) has a long electron spin relaxation time, T_{1e}, due to an orbitally nondegenerate ground state (11). However, several anion inhibitors bind to the metal (12–14) to yield a chromophore with low lying excited orbital states that lead to a very short T_{1e} (2, 11) and hence narrow NMR lines, as well as impart significant magnetic anisotropy to the metal ion, and hence large dipolar shifts to active site residues (1, 11).

The protocol for determining the magnetic axes is to search for the magnetic anisotropies and the rotation matrix that converts a crystal coordinate system into one that correctly predicts the observed dipolar shifts. Once this has been achieved, an ideal scenario would have the changes in dipolar shifts for conserved residues in point mutants or natural genetic variants interpretable in terms of modulation of the orientation of the axes if bonding ligands are perturbed. With or without perturbation of the magnetic axes and anisotropy, the observed dipolar shifts of the substituted residue can be interpreted in terms of orientation. Preliminary studies of numerous point mutants of metMbCN reveal that strong alteration in dipolar shift patterns are qualitatively interpretable solely in terms of change in the orientation of the magnetic axes, and that these changes can be interpreted in terms of steric constraints on the active site (15, 16).

In this report we present our initial results on the applications of modern one- and two-dimensional methods for assigning resonances in two five-coordinated adducts of bovine Co(II)CA (BCA II), i.e., nitrate and perchlorate (12, 17–20), and explore the prospects for determining the magnetic axes using the assigned resonances and the x-ray crystal coordinates of the five-coordinated NCS^- adduct of Zn(II)HCA II (21). Assignment will be pursued by a combination of one-dimensional NOE, as well as two-dimensional COSY and NOESY. In view of the limited utility of two-dimensional methods for de novo assignment, we will pursue assignments largely by one-dimensional NOEs and two-dimensional NOESY peaks on the basis of crystal coordinates. As the x-ray structures of HCA II(9) and its NCS^- adduct (21) are available at high resolution, we test and discuss, on the basis of the assignment, how the structure of the active site is perturbed by anion binding as well as how sensitive the dipolar shifts are to these changes.

MATERIALS AND METHODS

Bovine Carbonic Anhydrase II was purchased from Sigma Chemical Co. (St. Louis, MO) and used without further purification. Zinc(II) ions were removed by dialysis against solutions of pyridine 2,6-dicarboxylic acid (22) (5×10^{-2} M) in phosphate buffer (2×10^{-1} M) at pH 6.9, and the cobalt(II) derivatives were prepared by following spectrophotometrically the titration of the apoenzymes with a cobalt(II) sulfate solution.

All the ^1H NMR samples were 2–3 mM in Hepes buffer (20 mM) at pH 6.2–6.3. The D_2O samples were prepared by D_2O exchange using ultafiltration membrane. The anion concentrations were such as to completely form the final adducts ($\simeq$0.2 M).

The ^1H NMR spectra were recorded on Bruker AMX 600 (Bruker Spectrospin SRL, Milan, Italy), GEΩ 300 Nicolet NTC-360 (Nicolet Instrument Corp., Madison, WI), Bruker ACP 300 and Bruker MSL 200 spectrometers using a superWEFT (23) pulse sequence for suppressing the water signal. T_1 values were calculated by using either the inversion recovery (24) method (at 200 MHz) or the saturation recovery (25) method (at 300 MHz).

The ^1H NOE experiments were performed on the Nicolet 360 and on the Bruker ACP 300 using the same superWEFT pulse sequence, and they have been recorded using typical recycle times of 100–300 ms and selective saturation pulses of 0.01–0.002 W lasting 50–100 ms. They have been collected using the previously reported methodology (26). Some NOE experiments in water had been performed also with the Redfield (2 $\bar{1}$ 4 $\bar{1}$ 2) pulse sequence to avoid saturating the water signal (27).

The NOE values were analyzed with the following equation:

$$\eta_{ij} = \frac{\sigma_{ij}}{\rho_i}, \qquad (1)$$

where σ_{ij} is the cross-relaxation rate between protons i and j, and ρ_i is the selective relaxation rate of the proton on which the NOE effect is observed. The parameter σ_{ij} in turn is given by

$$\sigma_{ij} = \left[\frac{\mu_0}{4\pi}\right]^2 \frac{1}{10} \frac{\hbar\gamma^4}{r_{ij}^6} \left(\frac{6\tau_c}{1 + \omega_I^2\tau_c^2} - \tau_c\right). \quad (2)$$

For the analysis of the NOE data nonselective T_1's were used. This is a good approximation in the case of paramagnetic, fast relaxing signals (28–31).

The two-dimensional experiments were performed at 300 and 600 MHz with presaturation of the H_2O or the HDO signal during the recycle delay and the mixing times. NOESY (32) spectra were recorded using variable mixing times (15–80 ms) with a recycle time of 0.1–1 s. They were collected in the phase sensitive mode using the time proportional phase increment method (TPPI) (33). An array of 512 FIDs were collected using 512 or 1,024 data points each. Zero filling in the F1 dimension was applied to obtain a 1K × 1K 2D data point matrix. To the data the following weighting functions were applied:

$$\sin^2\left[\left(\pi - \frac{\pi}{\mathrm{SSB}}\right) \cdot \frac{t}{\mathrm{AQ}} + \frac{\pi}{\mathrm{SSB}}\right] \quad (3)$$

with SSB = 2, 3 or 4. COSY spectra have been recorded in Magnitude mode (34) (MCOSY). Also, for these experiments FIDs were collected with 1K data points; zero filling on the F1 dimension was applied. In this case the applied weighing function was

$$\sin^n \frac{\pi t}{\mathrm{AQ}}, \quad (4)$$

with n = 2 or 4. All the two-dimensional MCOSY maps were symmetrized. Experiments were also run with much faster repetition rates to improve the signal-to-noise ratio and then to detect broad signals. These spectra were recorded with 256 FIDs with 512 data points.

RESULTS

Cobalt(II) substituted BCA derivatives with perchlorate (Fig. 2 *A*) and nitrate (Fig. 2 *B*) yield ^{1}H NMR spectra with four signals well shifted downfield, plus numerous signals between 25 and −15 ppm. Signals *A*, *C*, and *D* disappear when the spectrum is recorded in D_2O. They are assigned to NH protons of the three histidines bound to the cobalt(II) ion (37). Signal *B* is due to the Hδ2 proton of His 119, which is bound through Nδ1 (Fig. 1). The correlation of resonances between the two adducts was achieved by following the averaged chemical shifts upon titrating the perchlorate adduct with nitrate. Hence, any assignment can be cross-correlated for the two adducts, and assignments of specific signals can be pursued on the derivative most suitable for the NMR experiment.

Because of the large bandwidth and consequent low digital resolution of a NOESY map of the complete spectrum, we initially identify protons in the ClO_4^- adduct in the 20 to −10 ppm window dipolarly coupled to the four extreme low-field signals by performing steady state NOE on signals *A–D*. Subsequent two-dimensional NOESY and MCOSY maps are recorded over the more reasonable 20 to −10 ppm window to establish the bond correlation and NOE properties of the signals which yield NOEs upon saturating the low-field peaks.

Fig. 3 shows the NOEs obtained by saturation (100 ms) of the paramagnetically shifted signals in Co(II)BCA

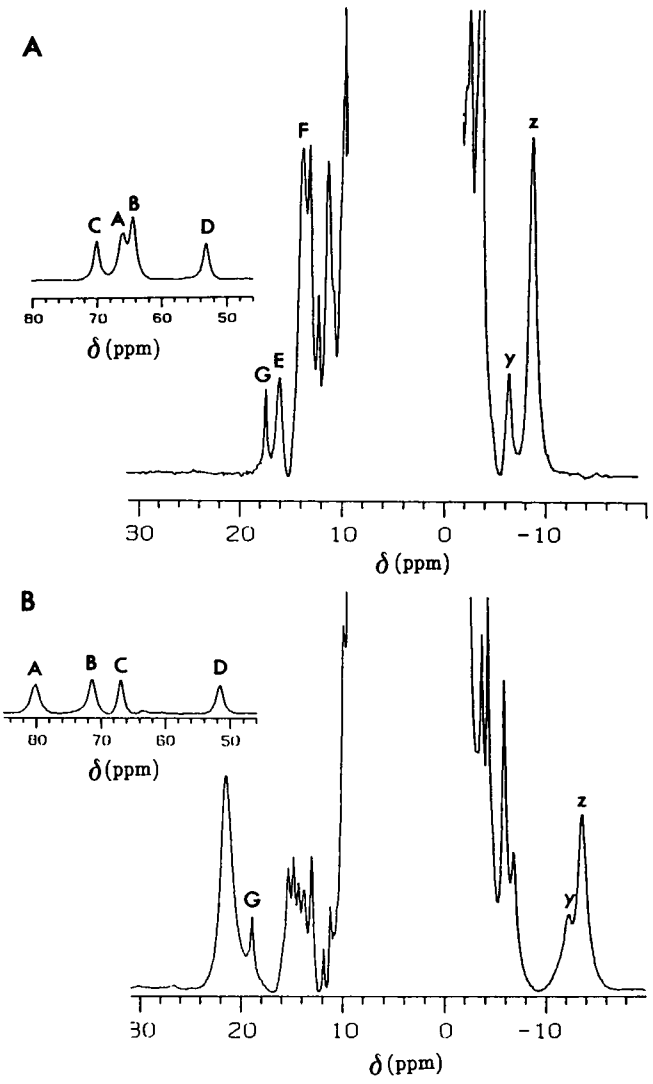

FIGURE 2 360 MHz 298 K ^{1}H NMR spectra in H_2O of the (*A*) ClO_4^- and (*B*) NO_3^- adducts of cobalt(II) substituted bovine carbonic anhydrase at pH 6.2–6.3 in 20 mM Hepes buffer.

II + ClO_4^-. The signals are labeled as in Table 1, where their assignment is also reported. Similar experiments were also performed on the nitrate adduct, in which the paramagnetically shifted signals are spread over a larger range. For the NO_3^- adduct, NOE is observed between signals *A* and *B*, as shown in Fig. 4. Therefore, signals *A* and *B* are due to the Hε2 and Hδ2 of His 119. The magnitude of the NOE (≃ −6%) is consistent with this assignment, using a τ_c of 15 ns as evaluated from the Stock-Einstein equation for a molecule of MW 30,000.

Saturation of signal *A* in the ClO_4^- adduct (Fig. 3 *A*) provides few NOEs in the 20 to −10 ppm region, of which the largest is to signal *G*, which is exchangeable. Saturation of signal *B* (Hε2 His–119) provides a rich set of connectivities (Fig. 3 *B*), to signals labeled *E*, *H*, *I*, *J'*, *J*, *J''*, *L*, *U*, *V*, and others. In contrast, saturation of signals *C* and *D* gives rise to fewer NOEs in the diamagnetic region.

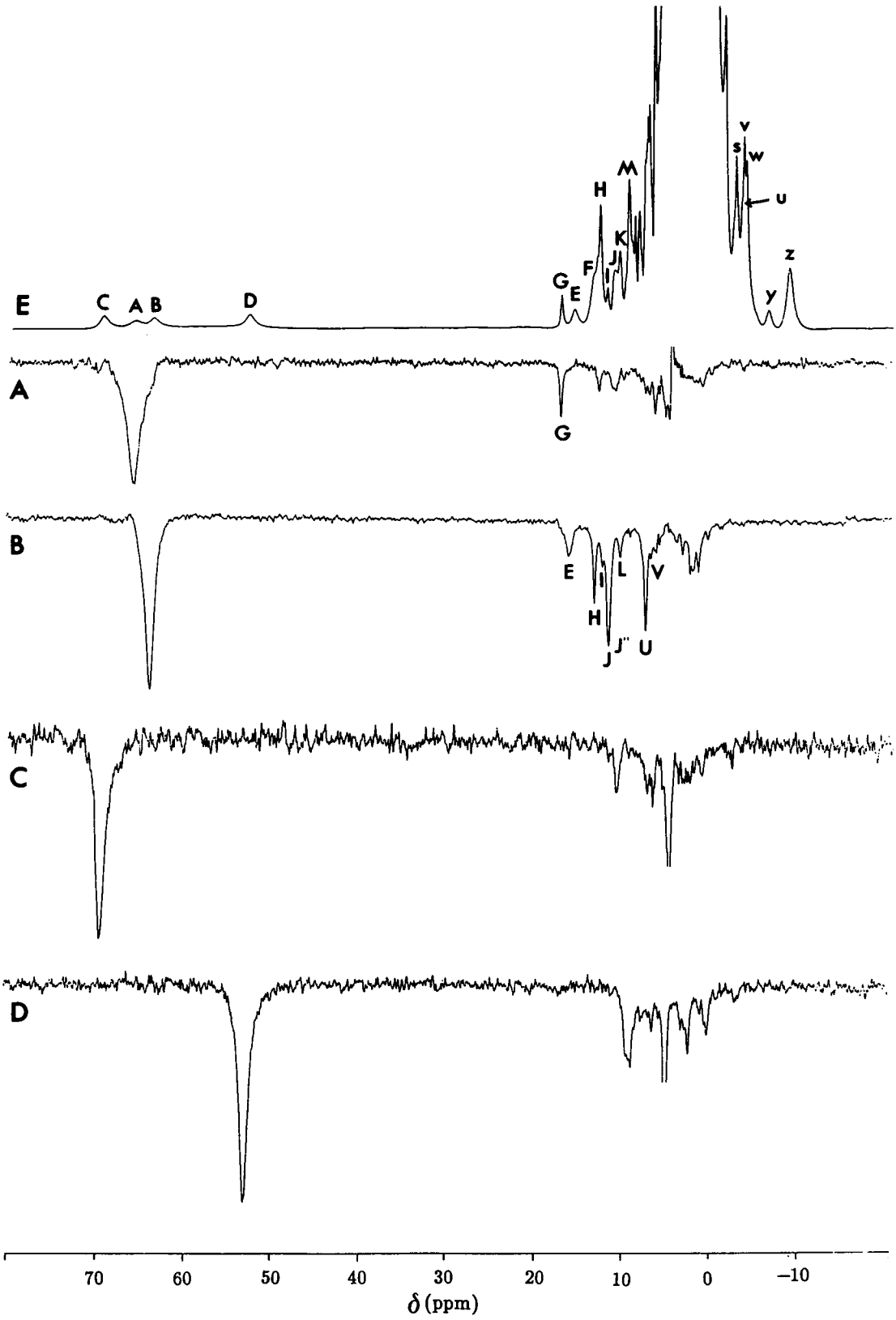

FIGURE 3 300 MHz 300 K ^{1}H NOE difference spectra of the ClO_4^- adduct of cobalt(II) substituted bovine carbonic anhydrase in H_2O obtained upon saturation (100 ms) of signal *A–D;* the reference spectrum (*E*) is also reported. The sample conditions are as in Fig. 2.

TABLE 1 Experimental and calculated[a] shifts for active site protons in cobalt(II) substituted carbonic anhydrase, and assignments of some ^{1}H NMR signals

Proton			Zn − H	F[b]	δ_{cal}	Ass.	δ_{obs}	T_1[c]
			Å		*ppm*		*ppm*	*ms*
A Nonligand protons with $\delta_{cal} > 15$ ppm and < -2 ppm								
Hδ1	His	107	7.45	0.09	17.43	G*	17.4	57
Hα	His	119	5.69	0.46	15.50	E*	16.0	22
NH	His	119	5.34	0.68	15.02			
Hβ	Phe	95	8.01	0.06	−2.21			
Hβ	Val	143	7.18	0.11	−2.43	u[d]		
CH_3	Val	207	9.09	0.03	−2.58	s*	−2.5	104
CH_3	Val	207	9.23	0.03	−2.73	v*	−3.4	85
Hα	His	96	6.39	0.23	−2.80			
CH_3	Val	143	7.21	0.11	−3.31	w[d]	−3.8	
Hα	Leu	198	6.56	0.20	−3.51			
CH_3	Ala	65[e]	6.71	0.19	−3.76			
NH	Phe	95	6.33	0.24	−3.82			
NH	Thr	199	4.96	1.05	−4.28			
CH_3	Thr	199	5.92	0.36	−8.82	z*	−8.4	18
Hζ2	Trp	209	5.49	0.57	−12.98			
Hη	Trp	209	4.07	3.46	−20.01			
OH	Thr	199	3.21	14.34	−50.71			
B Nonligand protons with $15 \leq \delta_{cal} \leq 10$								
CH_3	Thr	200	5.56	0.53	13.97	F*	13.8	10
Hγ2	Glu	117	6.11	0.30	13.82			
NH	Leu	120	7.08	0.12	12.92	I*	12.2	
NH	Ile	146[f]	8.33	0.05	12.67			
NH	Leu	118	8.01	0.06	12.50			
NH	Glu	106	7.73	0.07	12.11			
Hε	Gln	92	6.65	0.18	11.33			
OH	Thr	200	6.95	0.14	11.11			
Hη	Trp	5	8.13	0.05	10.92			
NH	His	107	8.19	0.05	10.87	H″	13.0	
NH	Thr	200	6.16	0.29	10.68			
Hβ1	Glu	117	6.18	0.28	10.27			
NH	Arg	246	7.32	0.10	10.17			
NH	Val	121	7.87	0.07	10.12			
C Protons of cobalt(II) ligands								
Hδ1	His	94	5.23	0.76	13.87	*D* (*C*)	52.4	14.6g
Hε1	His	94	3.49	8.61	31.54			
Hδ2	His	94	3.18	14.98	−92.96			
Hβ1	His	94	6.26	0.26	−4.00			
Hβ2	His	94	5.55	0.53	−13.24			
Hδ1	His	96	5.10	0.89	11.25	*C* (*D*)	69.0	9.5g
Hε1	His	96	3.13	16.61	29.66			
Hδ2	His	96	3.52	8.26	19.06			
Hβ1	His	96	6.34	0.24	2.08			
Hβ2	His	96	5.80	0.41	4.65			
Hε1	His	119	3.00	21.35	45.71			
Hε2	His	119	4.86	1.19	29.29	*A*	64.3	5.4g
Hδ2	His	119	5.09	0.90	23.09	*B*	63.4	5.7g
Hβ1	His	119	3.95	4.12	20.05			
Hβ2	His	119	3.19	14.73	43.53			
D Nonligand protons with $10 \leq \delta_{cal} \leq -2$[h]								
Hζ2	Trp	5	9.24	0.03	9.65			
Hζ3	Trp	5	9.63	0.02	9.91			
OH	Tyr	7	7.14	0.12	9.95			
Hη	Trp	16	8.69	0.04	9.36			
Hγ	Ser	29	10.53	0.01	1.26			
Hβ	Ser	29	8.39	0.04	−0.32			
Hβ	Ser	29	8.33	0.05	−1.07			
Hβ	Pro	30	7.89	0.06	1.27			
Hδ	Pro	30	7.94	0.06	2.38			
Hα	Pro	30	9.24	0.03	2.42			
Hδ2	His	64	6.77	0.16	9.20			
Hα	Ala	65[e]	8.82	0.03	0.45			
Hε	Phe	66	11.53	0.01	5.24			
Hδ	Phe	66	11.46	0.01	5.04			
NH	Phe	66	8.64	0.04	3.51			
Hδ2	Asn	67	6.94	0.14	5.86			
Hδ2	Asn	67	7.33	0.10	3.79			
Hβ	Asn	67	9.60	0.02	2.41			
Hα	Asn	67	8.72	0.04	2.52			
Hε	Gln	92	7.22	0.11	9.97			
Hα	Phe	93	7.15	0.12	5.66			
NH	His	94	5.92	0.36	7.03			
Hα	His	94	7.16	0.12	−1.11			
Hδ	Phe	95	8.80	0.03	3.59			
Hβ	Phe	95	7.84	0.07	−0.19			
Hα	Phe	95	5.65	0.48	−2.00			
NH	His	96	6.22	0.27	4.18			
Hε3	Trp	97	8.60	0.04	3.31			
Hζ3	Trp	97	8.37	0.05	1.52			
Hη	Trp	97	10.08	0.01	4.01			
NH	Trp	97	8.70	0.04	5.69			
Hβ	Ser	105	9.62	0.02	6.15			
Hα	Ser	105	8.47	0.04	6.98			
Hγ1	Glu	106	5.49	0.57	9.71			
Hγ2	Glu	106	6.63	0.18	4.61			
Hβ1	Glu	106	6.74	0.17	3.63			
Hβ2	Glu	106	6.24	0.26	6.88			
Hε1	His	107	7.16	0.12	4.89			
Hγ1	Glu	117	7.87	0.07	7.63			
Hβ2	Glu	117	7.89	0.06	6.24			
NH	Glu	117	8.13	0.05	9.55			
Hα	Glu	117	8.42	0.04	7.82			
Hγ	Leu	118	8.32	0.05	4.49			
Hβ	Leu	118	8.92	0.03	4.34			
Hα	Leu	118	6.57	0.19	6.98			
Hα	Leu	120	8.12	0.05	6.36			
CH_3	Val	121	8.09	0.06	1.32			
CH_3	Val	121	5.48	0.58	4.15			
Hβ	Val	121	7.79	0.07	3.63			
CH_3	Val	143	5.61	0.50	−1.00			
NH	Val	143	9.92	0.02	6.87	*b*[d]	6.2	
Hα	Val	143	8.55	0.04	3.69	*j*[d]	0.1	
Hα	Gly	145	8.11	0.06	7.14	*V*	6.8	
Hα	Gly	145	7.39	0.10	9.37	*J*	11.2	
Hγ	Ile	146[f]	10.41	0.01	3.53			
Hβ	Ile	146[f]	10.21	0.01	4.11			
Hα	Phe	147	10.64	0.01	6.69			
Hα	Gly	196	11.36	0.01	1.72			
NH	Ser	197	10.06	0.02	5.12			
Hα	Ser	197	10.62	0.01	1.97			
CH_3	Leu	198	7.49	0.09	−1.18			
CH_3	Leu	198	9.27	0.02	1.51			
Hβ	Leu	198	6.97	0.14	1.10			

TABLE 1 (continued)

Proton			Zn − H	F[b]	δ_{cal}	Ass.	δ_{obs}	T_1[c]	Proton			Zn − H	F[b]	δ_{cal}	Ass.	δ_{obs}	T_1[c]
			Å		*ppm*		*ppm*	*ms*				Å		*ppm*		*ppm*	*ms*
D Nonligand protons with $10 \leq \delta_{cal} \leq -2$[h] (continued)																	
NH	Leu	198	9.38	0.02	5.80				Hα	Val	207	11.60	0.01	2.42	*g**	2.4	
Hβ	Thr	199	5.49	0.57	1.99				Hδ1	Trp	209	10.41	0.01	4.48			
Hα	Thr	199	6.89	0.15	1.33				Hε1	Trp	209	8.16	0.05	3.96	*d*[d]	3.0	
Hβ	Thr	200	7.54	0.09	9.92	*M**	9.8		Hζ3	Trp	209	5.97	0.34	7.14			
Hα	Thr	200	7.77	0.07	7.88				Hδ	Asn	244	7.24	0.11	1.50			
Hδ	Pro	201	9.73	0.02	6.16				Hδ	Asn	244	8.88	0.03	3.26			
Hδ	Pro	201	9.58	0.02	5.79				Hα	Trp	245	6.97	0.14	6.31			
Hβ	Val	207	9.85	0.02	−1.34	*p**	−1.1		Hβ	Arg	246	7.92	0.06	2.39			

* Used in the search for the χ-tensor orientation. [a]The diamagnetic shift values for the various kinds of protons have been taken from literature[35]. The associated errors may be as large as ±2 ppm and even larger for NH protons[36]. [b]F represent a parameter proportional to $1/r^6$ and therefore to the signal linewidth and T_1^{-1}. F = 1 corresponds to a distance of 5 Å, which is approximately the metal proton-distance for signals *A* − *D*. [c]Nonselective T_1 values have been measured at 300 MHz using the saturation recovery method and at 200 MHz (where indicated) using the inversion recovery method. In both cases, exponential behavior was assumed. The estimate errors are always within 10%. [d]A possible, but not unique, assignment consistent with the dipolar susceptibility tensor orientation and with NOESY connectivities. [e]In BCA II Ala is replaced by Ser. [f]In BCA II Ile is replaced by Val. [g]Measured at 200 MHz[20]. [h]Table 1 *D* only shows protons which either are located within in an 8-Å radius sphere from the metal ion or experience a calculated dipolar shift larger than ±2 ppm.

Fig. 5 *A* illustrates MCOSY maps of Co(II)BCA II + ClO_4^-, collected at a rate of 20 s^{-1} (with 7,200 scans) that emphasizes weak cross-peaks between fast relaxing, broad resonances, but produces too intense a diagonal to allow detection of peaks close to the diagonal. The MCOSY map in Fig. 5 *B* was collected at a more conventional rate of 1.5 s^{-1} (only 700 scans) which does not have the sensitivity to detect cross-peaks between some of the broad resonances, but clearly shows cross-peaks closer to the diagonal.

Among the signals dipolarly downfield shifted, scalar connectivities have been observed between signal *F* and the composite signal *M* (Fig. 5 *A*) and between the composite signal *J* and *V* (Fig. 5 *B*).

Among the upfield shifted signals, some typical patterns of amino acid residues are clearly detectable. Signals *s* and *v* are two CH_3 groups which are scalarly coupled with signal *p*. In turn, *p* is coupled with a signal at 2.4 ppm (*g*) (Fig. 5 *B*). This pattern identifies a valine residue. The shift values, their temperature dependence, as well as the T_1 values of the CH_3 groups suggest that this residue is only weakly interacting with the paramagnetic metal ion.

Fig. 6 *B* shows a NOESY map at 300 MHz of the Co(II)BCA II + ClO_4^- adduct in H_2O in the region 20/−10 ppm with a mixing time of 15 ms. With such short mixing time, only primary dipolar connectivities are detected.

The map is quite rich in cross-peaks. In particular, connectivities are observed between signals which are also coupled with the paramagnetically shifted signals. Among the many connectivities, signal *G* gives cross-peaks with *H″*; the broad signal *E* gives an intense cross-peak with *I*, signal *F* gives a cross-peak with the composite signal *M*. In the upfield region of the spectra the NOESY pattern of the valine residue formed by *v*, *s*, *p* and *g* is observed in a NOESY experiment with a mixing time of 80 ms (Fig. 7 *A*). Two intense cross-peaks are also observed between *m* and *p* and *m* and *s* (Fig. 7 *B*). Signals

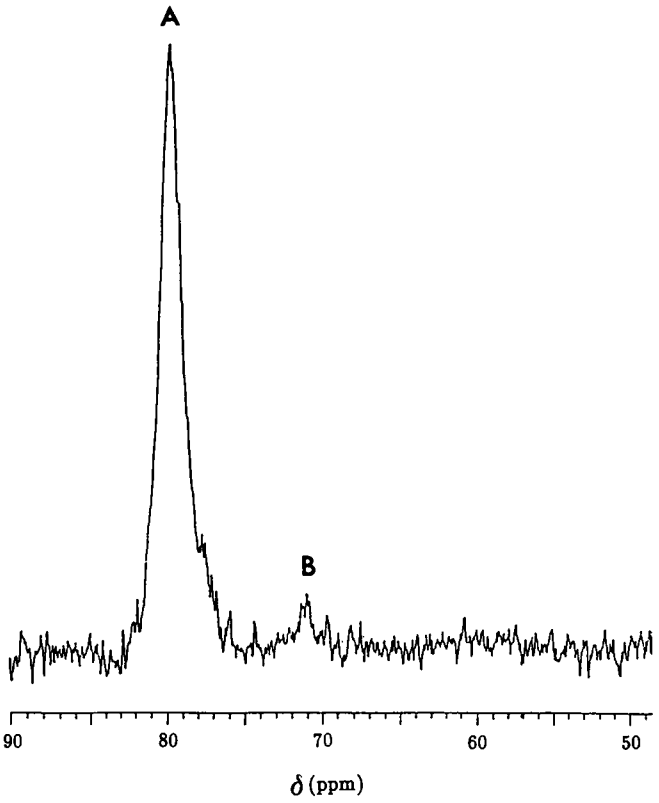

FIGURE 4 360 MHz 298 K ^{1}H NOE difference spectrum (reported as positive peaks) of the NO_3^- adduct of cobalt(II) substituted bovine carbonic anhydrase obtained upon saturation of signal *A*.

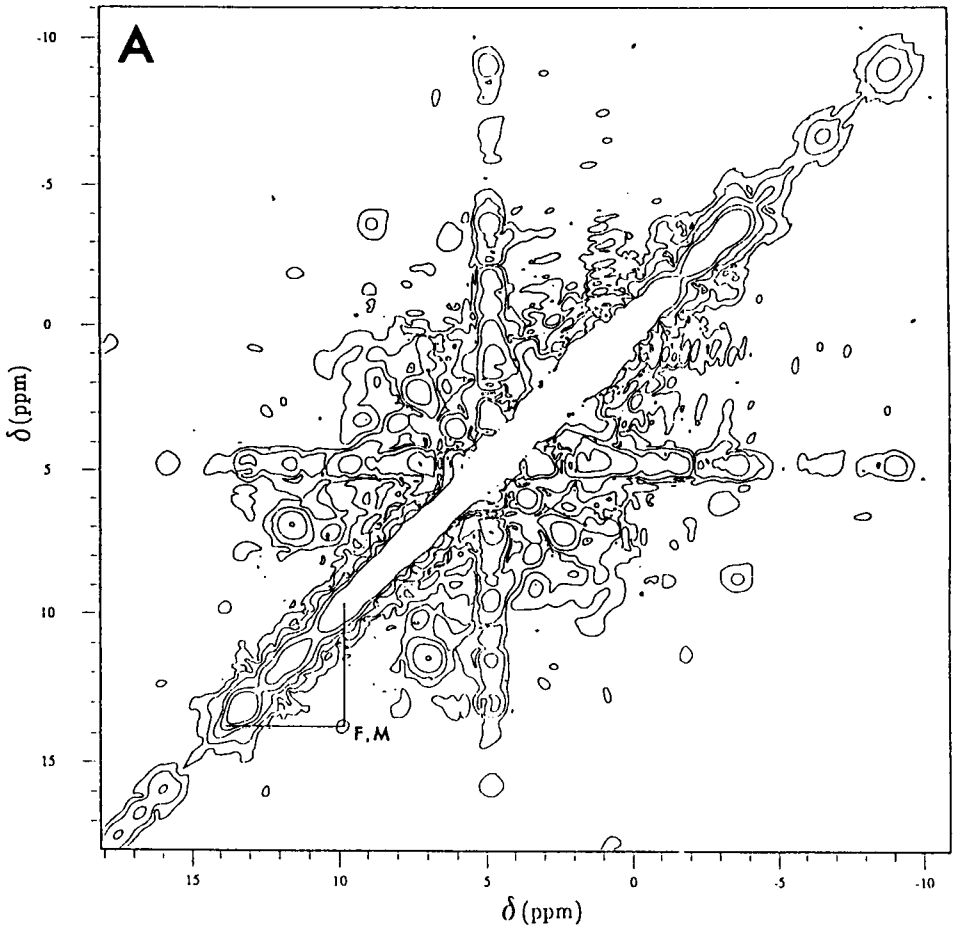
A
-10
-5
0
5
10
15
δ (ppm)
F, M
15
10
5
0
-5
-10
δ (ppm)

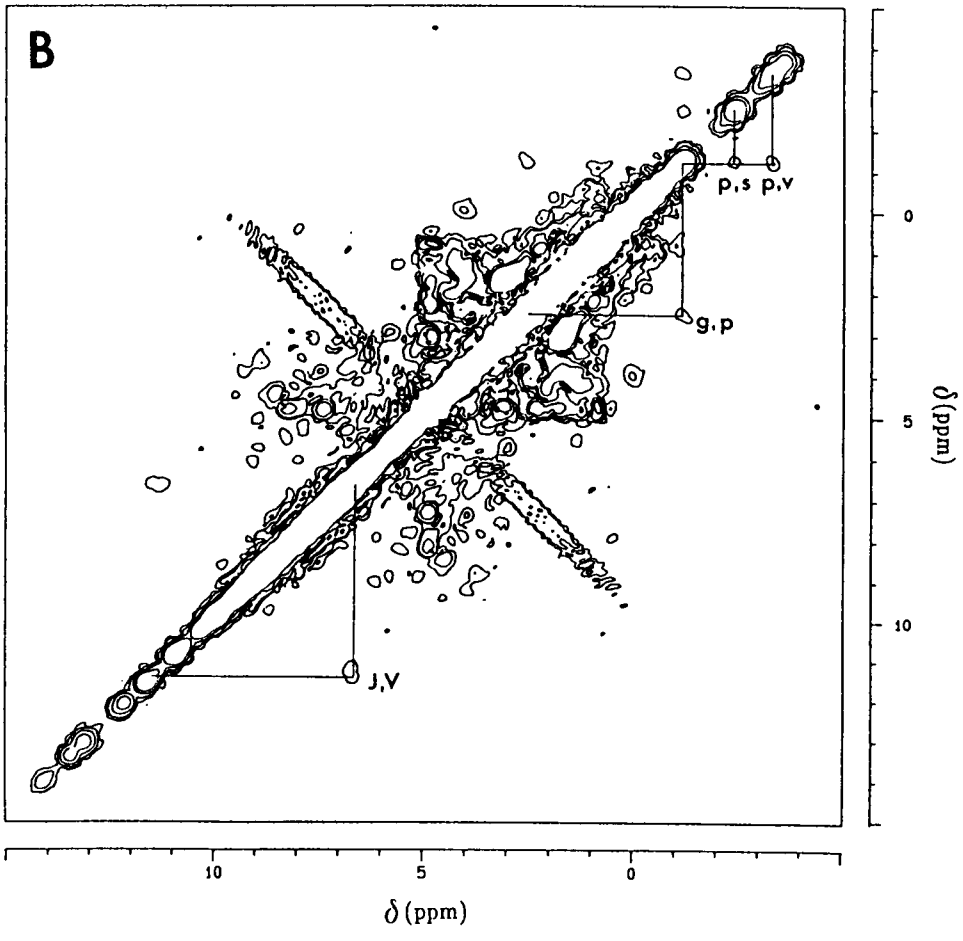
B
p, s
p, v
g, p
J, V
10
5
0
δ (ppm)
0
5
10
δ (ppm)

p, *s*, and *v* also give a large number of NOESY peaks with other signals in the diamagnetic region. Signal *w* gives cross-peaks with *v*, *u*, *s*, *j*, and *e*.

At much faster repetition rates, cross-peaks between the broad, upfield, CH_3 signal (*z*) are also detected with signals at 0 ppm and 1.7 ppm (Fig. 6 *A*). It is important, however, to note that beneath the broad signal *z*, other two signals are present, as evidenced by temperature dependence and titration.

MCOSY and NOESY maps have also been recorded at 600 MHz (data not shown). At such high magnetic field, due to the large contribution of Curie relaxation to the linewidth, the broad signals are not detected, but the maps confirm the connectivities observed among the slow relaxing signals and the increased resolution allows us to detect a few more patterns in the diamagnetic region, whose discussion is beyond the scope of the present research.

ASSIGNMENT OF THE SPECTRA

Table 1 reports a list of active site protons together with their distances from the metal ion and their predicted shifts (see later). The observed shifts for the protons assigned in this section are also reported.

For the analysis of the spectra we use the x-ray structures of the human II isoenzyme (9) and that of its NCS^- adduct, which is five-coordinated (21). Binding of NCS^- induces only very small changes in the arrangement of the residues in the active cavity. The NMR spectra of some anion adducts of human II and bovine isoenzymes are very similar (18). We, therefore, use with some confidence these structures as a starting point for the assignment of the NMR spectra, but also try to use the NMR information as a feedback to detect possible modest structural modifications due to anion binding.

Besides the far downfield histidine ring protons, the spectra of the anion derivatives show two CH_3 signals, one downfield and one upfield, which experience large line width and short T_1 values, indicating that they are close to the metal ion (signals *F* and *z* in Fig. 3 *E*). They do not experience any connectivity with the dipolarly shifted signals, and very few with other signals. This suggests that they do not belong to Val or Leu residues (see also later). We propose that these signals are due to the CH_3 groups of Thr 199 and Thr 200, which are in the active cavity. They are quite isolated from the other assigned signals, consistent with the lack of NOE connectivities. In addition, we propose that the upfield signal (*z*) is due to Thr 199 (Table 1 *A*) and the downfield signal (*F*) is due to Thr 200 (Table 1 *B*) as this signal is not present in the anion adducts of human CA isoenzyme I (38), where this residue is replaced by a His (39). This signal *F* gives MCOSY and NOESY cross-peak with signal *M* (Fig. 5 *A*) which could be assigned as its β-proton (Table 1 *D*).

Signal *A* (Hϵ2 His 119) provides NOE with the exchangeable signal *G* (Fig. 3 *A*). The real nature of the NOE effect has been checked through Redfield experiments, i.e., without saturation of the water signal. In addition, increasing the temperature determines a decreasing in the extent of the NOE effect, ruling out the possibility of detection of a saturation transfer effect. The only candidate for signal *G* is the Hδ1 of His 107, which is at 2.7 Å from Hϵ1 of His 119 (Table 1 *A*). No other exchangeable protons are close to the NH of His 119, in such a way to provide detectable NOE. Signal *G* in turn gives a NOESY cross-peak with signal *H″* (Fig. 6 *B*); the latter is heavily overlapped with signal *H* and *H′* in H_2O, whereas in D_2O at least one of the three disappears. If *H″* is exchangeable, a good candidate is the peptide NH of the His 107 (Table 1 *B*).

Signal *B* (Hδ2 His 119) provides a wealth of strong NOEs in the 20–0 ppm range (Fig. 3 *B*). Indeed, on the basis of the x-ray structure, four protons are within 2.4–2.6 Å from Hδ2 of His 119. These are Hα His 119 (5.7 Å), Hγ2 Glu 117 (6.1 Å), Hζ3 Trp 209 (6.0 Å) and Hα1 Gly 145 (7.4 Å), where the numbers in parenthesis indicate the distance from the metal ion. The presence of four protons at essentially the same distance from Hδ2 of His 119 makes the assignment of the NOEs from signal *B* difficult in the absence of additional information. Even the two-dimensional MCOSY and NOESY maps (Figs. 5, 6, and 7) do not yield connectivity patterns that allow unambiguous assignment of any of the major NOEs from signal *B*. According to the linewidths, an obvious choice would be to assign signal *E* as the Hα proton of His 119, which is the closest to the metal ion. This assignment is confirmed by preliminary data on a sample selectively deuterated on α and ring positions of histidines (unpublished observations). The ClO_4^- adduct of the cobalt derivative of this sample lacks a broad signal at the same position of signal *E*. We can therefore assigne with confidence signal *E* as the α proton of His 119. Signal *I*, giving a strong NOESY cross peak with *E* is therefore assigned as the peptide NH proton of Leu 120.

Among the other three protons in the immediate neighborhood of Hδ2 of His 119, Hα1 of Gly 145 should be the sharpest and should certainly give rise to observable COSY and NOESY cross-peaks with its geminal protons. By this argument, we can rule out signal *H* as a

FIGURE 5 (*A*) 300 MHz 298 K MCOSY spectrum of the ClO_4^- adduct of cobalt(II) substituted carbonic anhydrase at pH 6.0–6.2 in Hepes buffer 20 mM in D_2O; repetition rate 20 s^{-1}. (*B*) 300 MHz 300 K MCOSY spectrum of the ClO_4^- adduct of cobalt(II) substituted carbonic anhydrase in H_2O; repetition rate 1.5 s^{-1}. The sample conditions are as in Fig. 2.

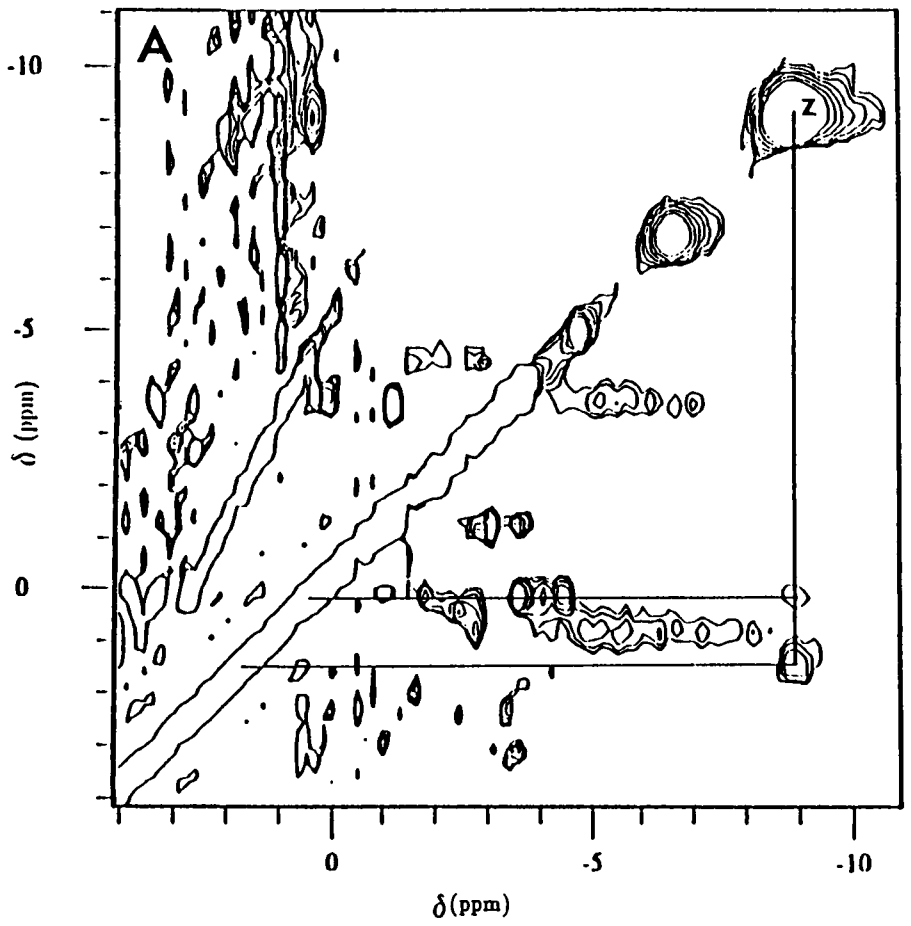
A
-10
-5
0
δ (ppm)
Z
0
-5
-10
δ(ppm)

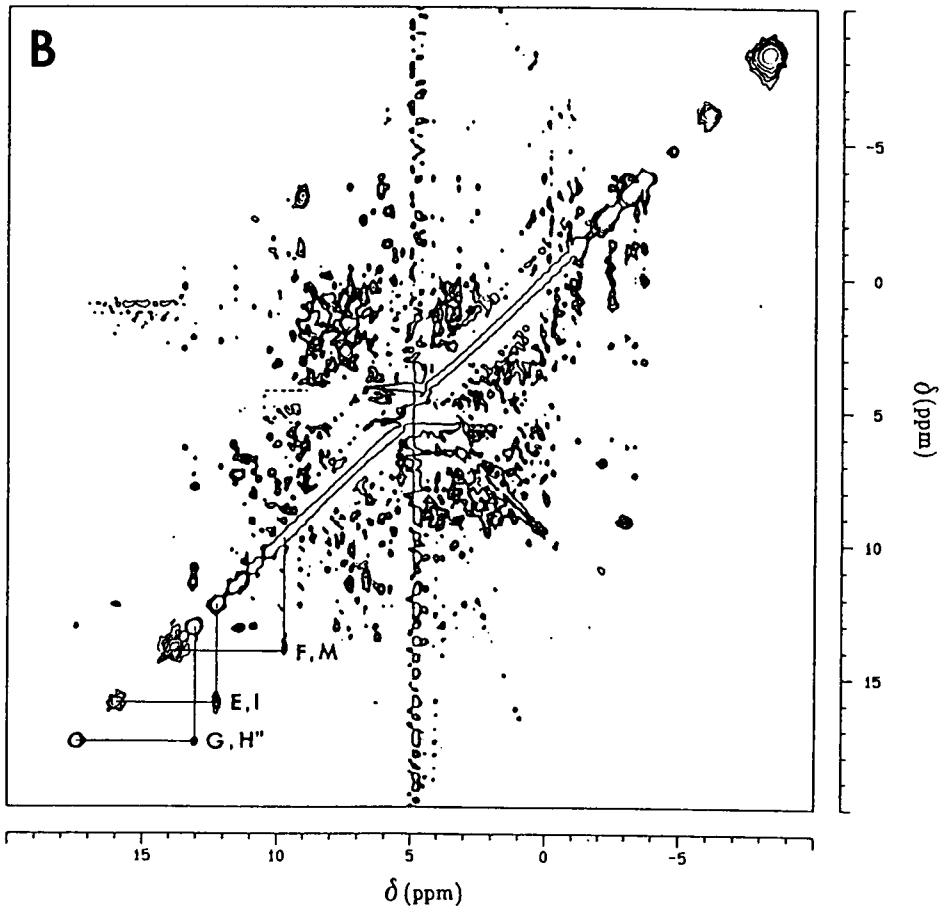
B
F, M
E, I
G, H"
15
10
5
0
-5
δ (ppm)
-5
0
5
10
15
δ(ppm)

candidate. On the other hand, there is a strong scalar and dipolar coupling between *V* and one component of *J* (Fig. 5 *B*), suggesting that these are geminal protons. They could thus, correspond to Hα2 and Hα1 of Gly 145, respectively. However, the possibility that signal *U*, which is also sharp and gives a strong NOE upon irradiation of *B*, has NOESY and MCOSY cross-peaks hidden in a more crowded region of the spectrum cannot be ruled out. We, therefore, consider the assignment of *J* as Hα1 of Gly 145 as only tentative.

NMR characterization has been also performed on the nitrate adduct whose spectrum shows similar features with those of perchlorate. Saturation of signals *A* and *B* gives NOE patterns similar to those observed in the case of perchlorate, i.e., *A* is connected with signal *G*. *B* gives NOE with signal *E* and with a few other signals at ~15–12 ppm, which can be correlated with the signals of the perchlorate adduct. The slopes, obtained by plotting the variation of shifts in the difference spectra of NOE experiments, over a fixed temperature interval, versus $1/T$, have the same relative trend in the two adducts.

The two CH_3 signals, one downfield and one upfield, which experience fast relaxation (signal *F* and *z*) are also present in the spectrum of the nitrate adduct, and their correspondence with the signal in the ClO_4^- adduct has been established by titrating the perchlorate adduct with nitrate. This experiment has also allowed us to correlate a few other signals.

The NOESY map (data not shown) reveals the presence of the typical pattern for valine among the signals *p*, *s*, and *v*, which are also correlated with those of the perchlorate adduct.

The T_1 values listed in Table 1 for the perchlorate adduct deserve some comments. The T_1 values of the signals of protons of residues directly coordinated to the metal ion are shorter in the case of the perchlorate adduct compared to those of the nitrate adduct, measured previously (18). This can be the result, in the latter case, of a shortening of the electron relaxation time, T_{1e}, which in such systems is the correlation time for the dipolar interaction with the unpaired electrons responsible for nuclear relaxation. A shorter T_{1e} is indicative of a more five coordinated character of the nitrate adduct, as also suggested by the electronic spectra. Estimation of T_{1e} is not straightforward, as the T_1 values of ligands of the metal ion are affected by sizable ligand centered effects due to delocalization of the unpaired spin density on the ligand rings. Also, the T_1 values of the CH_3 groups can be affected by internal mobility. In the case of the perchlorate adduct, by considering the T_1 value of signal *E* assigned as Hα of His 119, a T_{1e} of 2.0×10^{-12} s can be estimated for the cobalt(II) ion.

In the case of the nitrate adduct such signal is not isolated and its T_1 cannot be determined. However, from the ratio between the T_1 values of the γCH_3 signal of Thr 199 in the two adducts, a T_{1e} of about 1.3×10^{-12} s can be estimated for the cobalt(II) ion in the nitrate adduct.

Inspection of Table 1 shows that the T_1 values of the CH_3 signals identifying a valine residue are relatively long. This suggests that the valine identified by signals *s*, *v*, *p*, and *g* may not be very close to the metal ion, but it should still sense some hyperfine interaction to induce some dipolar shift. The possible candidates for this valine are: Val 121, 143 and 207. Among these, both Val 121 and 143 have at least one CH_3 group too close to the metal ion to have such a long T_1 value. Therefore from T_1 values and the distance from the metal ion we tentatively assign the upfield valine as Val 207 (Table 1, *A* and *D*). This assignment is consistent with the lack of NOE connectivities from this valine and the assigned signals, which are all close to Hδ2 of His 119 or belong to the hydrophilic side of the cavity.

The T_1 values of the other assigned signals are in qualitative agreement with the proton-metal distances of the x-ray structure, thus, further supporting the assignment.

DIPOLAR SHIFT CALCULATIONS

To determine the magnitude and the orientation of the principal axes of the magnetic susceptibility tensor in these five-coordinate adducts of cobalt(II) carbonic anhydrase, dipolar shift calculations have been performed for the signals of protons of noncoordinated residues assigned in this research and reported in Table 1.

The shift values of the protons in the perchlorate adduct are consistent with a magnetic susceptibility tensor whose orientation within the molecular frame is reported in Fig. 8. The axes make angles of 39°, 32°, and 164° with the Co—N(His 94), Co—NCS^- and Co—N(His 119) ligands respectively. The chromophore can, thus, be regarded as a distorted trigonal bipyramid whose *z* axis is roughly along the Co—N(His 119) bond or as a distorted square pyramid whose *z* axis is roughly parallel to the Co—N(His 94) bond. The expected and calculated shifts are reported in Table 1. The agreement between the experimental and calculated values is reasonably good.

The calculated magnetic susceptibility anisotropies for the choice of the *z* axis close to the Co—N(His 119) bond are $\Delta\chi_{ax} = -6.4 \times 10^{-8}$ m^3 mol^{-1} and $\Delta\chi_{eq} = 2.4 \times 10^{-8}$ m^3 mol^{-1}. The large $\Delta\chi_{eq}$ value indicates a sizable

FIGURE 6 (*A*) Upfield portion of the 300 MHz 298 K NOESY spectra of the ClO_4^- adduct of cobalt(II) substituted carbonic anhydrase. Repetition rate 10 s^{-1}, mixing time 15 ms in D_2O. The sample conditions are as in Fig. 5 *A*. (*B*) 300 MHz 300 K NOESY spectrum of the ClO_4^- adduct of cobalt(II) substituted carbonic anhydrase in H_2O. Repetition rate 10 s^{-1}, mixing time 15 ms. The sample conditions are as in Fig 2.

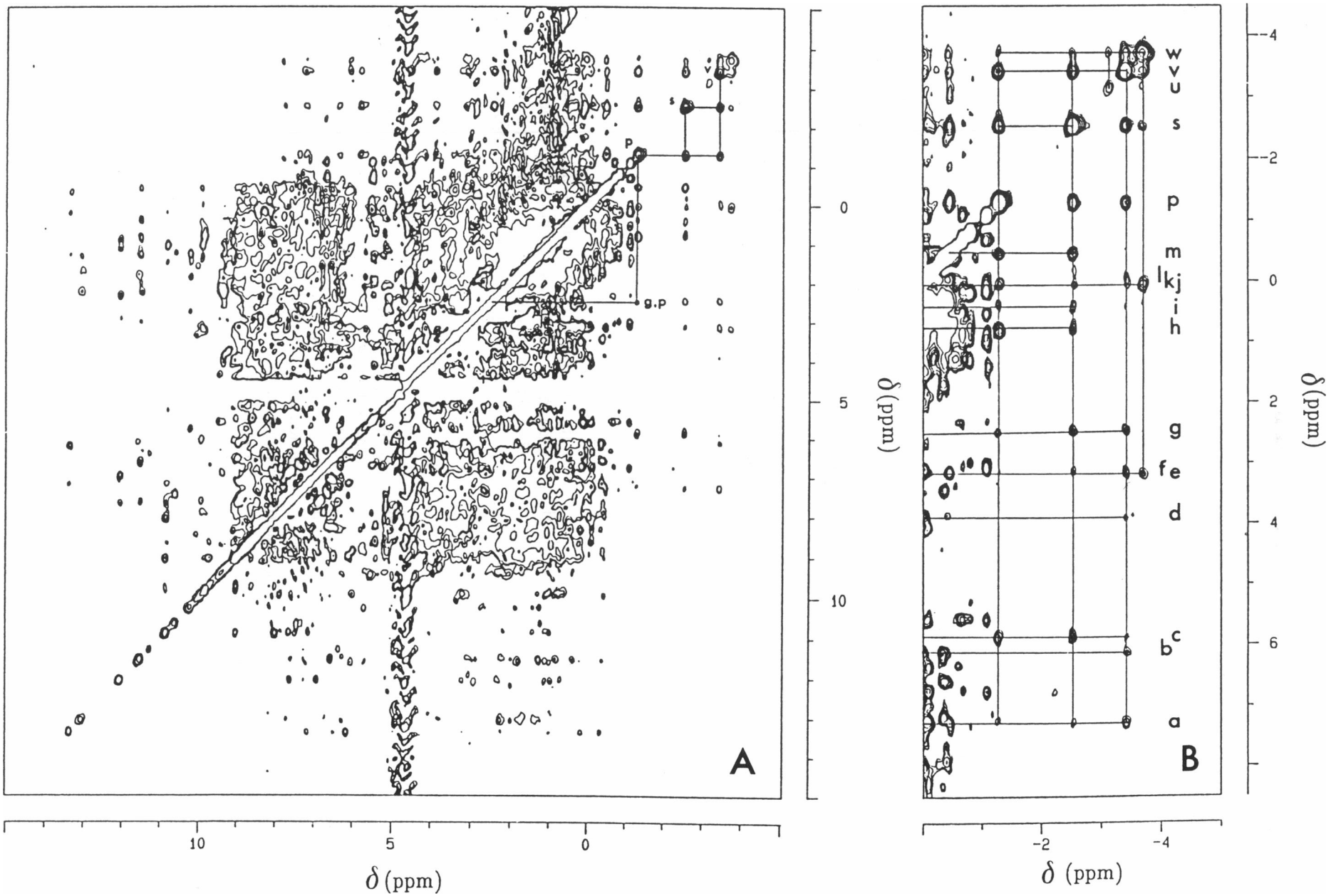

FIGURE 7 (*A*) 300 MHz 300 K NOESY spectra of the ClO_4^- adduct of cobalt(II) substituted carbonic anhydrase in H_2O. Repetition rate 1.7 s^{-1}, mixing time 80 ms (*B*) Expansion of the right hand side of (*A*). The sample conditions are as in Fig. 2.

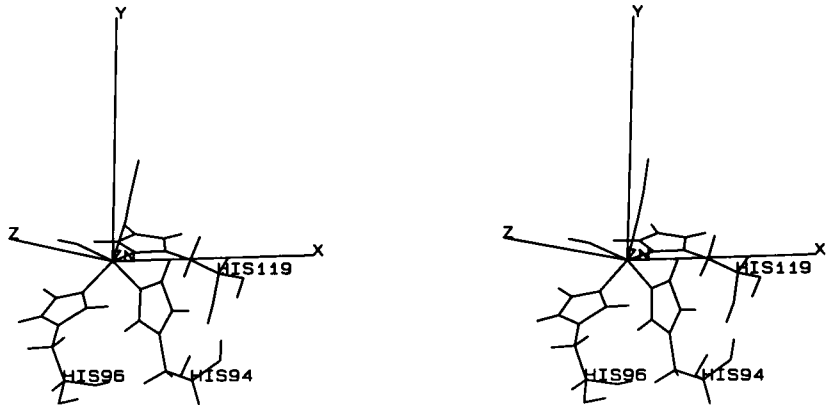

FIGURE 8 Stereoview of the orientation of the magnetic susceptibility tensor within the active site of HCA II + NCS (21). The angles of the principal axes with the closest metal ligand bonds are reported in the text.

rhombicity of the χ tensor in this derivative, consistent with the low actual symmetry of the chromophore.

The above orientation of the tensor was used to reproduce the shifts in the nitrate adduct, by adjusting the values of $\Delta\chi_{ax}$ and $\Delta\chi_{eq}$. The shifts for the assigned signals in the nitrate adduct are calculated with reasonably good agreement but with larger magnetic susceptibility anisotropy parameters ($\Delta\chi_{ax} = -9.5 \times 10^{-8}$ m^3 mol^{-1}, $\Delta\chi_{eq} = 5.2 \times 10^{-8}$ m^3 mol^{-1}). This is in complete agreement with what already discussed about the T_1 values. A larger magnetic susceptibility anisotropy as well as a shorter electron relaxation time T_{1e} is indicative of a larger five coordination character of the nitrate adduct with respect to the perchlorate one.

Table 1 *C* reports the calculated dipolar shifts for the cobalt ligand protons. The values for the signals *A–D* are all positive (i.e., downfield shifts) and much smaller than the experimental values. This is nicely consistent with relatively large and positive contact shift contribution. In addition, if the calculated dipolar shifts are subtracted from the experimental ones, very similar contact shifts are obtained for the four downfield shifted signals. We, thus, learn that the binding of the three histidines is very similar from the electronic point of view and presumably most of the spreading of the ^{1}H NMR signals, which is even larger in other anion derivatives (unpublished observations), is due to dipolar shift contribution.

Table 1 also reports the calculated shifts for all the protein protons which are closer than 8 Å to the metal ion or experience a calculated dipolar shift larger than ±2 ppm. As it can be seen, most are predicted to fall under the diamagnetic envelope and therefore are not easily detected. Among the few that are calculated outside the diamagnetic envelope some have a too large line width to be detected (Hη and OH of Trp 209 in Table 1 *A*, all the bound histidines protons in an orto-like position with respect to the coordinated nitrogen and the βCH_2 protons of His 199 in Table 1 *C*) or to be resolved from other sharper signals (Tables 1, *A* and *B*) and some others might be accidentally beneath other signals (as, for example, the βCH_2 protons of His 94 which experience also some positive contact shift) if a reasonable uncertainty is associated with their calculated shift values. For all the others a plausible assignment consistent with experimentally observed shifts and NOESY connectivities can be found.

Some of the latter tentative assignments are reported in Table 1. They should only be considered as further evidence of internal consistencies of the present choice of the dipolar susceptibility tensor and may not be unequivocal.

CONCLUSIONS

Two-dimensional methods, in conjunction with solution one-dimensional NOE experiments, have proven surprisingly useful for unraveling assignments even on such a large and strongly ($S = 3/2$) paramagnetic enzyme with lines as broad as 400 Hz. It is noted however that two-dimensional maps over a wide range of conditions (repetition rates, mixing times, temperature) must be collected to obtain meaningful information. The data presented herein constitute only the initial stage of a broader project aimed at assigning resonances in molecules of this type, but clearly illustrate the great promise of the two-dimensional method for providing assignments of particularly strongly hyperfine shifted lines.

The present study has allowed the assignment of the isotropically shifted signals and of a set of signals due to protons present in the active cavity and interacting with the paramagnetic center. This assignment has shown the similarities in the structures of two inhibitor derivatives, as a result of similar binding behavior.

The assignment of some signals which experience only pseudocontact shifts has allowed us to obtain information on the magnetic anisotropy of these systems and to estimate the orientation of the principal axes of the anisotropy tensor within the molecular coordinates.

We have also shown that NMR spectra of different adducts can be qualitatively accounted for by changing

the $\Delta\chi$ values, while maintaining the same orientation of the magnetic anisotropy tensor in the molecular frame. This is a quite relevant result as it will allow us to interpret more easily and quickly the spectra of other inhibitor adducts as well as of mutants of CA. It is worth noting that the dipolar shifts of several noncoordinated residues are sizably different in the two adducts, and yet the two χ tensor are rather similar. This finding gives an idea of how sensitive the dipolar shifts are to small geometric changes.

The present data allow us to propose that the structures of the two inhibitor adducts are similar as a result of a similar arrangement of the inhibitor molecule, and similar to that of the NCS^- derivative, whose x-ray structure is available (21). As already proposed (12), we have gained further evidence that both adducts are pentacoordinated with a water molecule coordinated to the metal ion, as in the NCS^- adduct.

This research was supported by grants from the National Science Foundation, grants DMB-88-03611 and DMB-91-04018, and from the Italian C.N.R. R. Pierattelli is grateful to Bruker Spectrospin Italiana s.r.l. for a research fellowship.

Received for publication 2 December 1991 and in final form 17 April 1992.

REFERENCES

1. Bertini, I., and C. Luchinat. 1986. NMR of paramagnetic molecules in biological systems. Benjamin/Cummings, Menlo Park, CA.
2. Banci, L., I. Bertini, and C. Luchinat. 1991. Nuclear and Electron Relaxation. The Electron Nucleus Hyperfine Coupling in Diluted Systems. VCH Publishers, Weinheim, Germany.
3. Ernst, R. R., G. Bodenhausen, and A. Wokaun. 1987. Principles of Nuclear Magnetic Resonance in One and Two Dimensions. Oxford University Press, London.
4. Emerson, S. D., and G. N. La Mar. 1990. Solution structural characterization of cyanometmyoglobin: resonance assignment of heme cavity residues by two-dimensional NMR. *Biochemistry.* 29:1545–1556.
5. Yu, L. P., G. N. La Mar, and K. Rajarathnam. 1990. ^{1}H NMR resonance assignment of the active site residues of paramagnetic proteins by 2D bond correlation spectroscopy: metcyanomyoglobin. *J. Am. Chem. Soc.* 112:9527–9534.
6. De Ropp, J. S., L. P. Yu, and G. N. La Mar. 1991. 2D NMR of paramagnetic metalloenzymes: cyanide-inhibited horseradish peroxidase. *J. Biomol. NMR.* 1:175–190.
7. Bertini, I., and C. Luchinat. 1983. An insight on the active site of zinc enzymes through metal substitution. *In* Metal Ions in Biological Systems. H. Sigel, editor. Marcel Dekker, Inc., New York. 101–156.
8. Bertini, I., C. Luchinat, and M. S. Viezzoli. 1986. Metal substitution as a tool of the investigation of zinc proteins. *In* Zinc Enzymes. I. Bertini, C. Luchinat, W. Maret, and M. Zeppezauer, editors. Birkhauser, Boston. 27–47.
9. Eriksson, A. E., T. A. Jones, and A. Liljas. 1989. Refined structure of human carbonic anhydrase II at 2.0 A resolution. *Proteins.* 4:274–282.
10. Coleman, J. E. 1973. Carbonic anhydrase. *In* Inorganic Biochemistry. Vol. 1. G. L. Eichhorn, editor. Elsevier, New York. 488–548.
11. Bertini, I., and C. Luchinat. 1985. High spin cobalt(II) as a probe for the investigation of metalloproteins. *Adv. Inorg. Biochem.* 6:71–111.
12. Bertini, I., G. Canti, C. Luchinat, and A. Scozzafava. 1978. Characterization of cobalt(II) bovine carbonic anhydrase and of its derivatives. *J. Am. Chem. Soc.* 100:4873–4877.
13. Bertini, I., and C. Luchinat. 1983. Cobalt(II) as a probe of the structure and function of carbonic anhydrase. *Acc. Chem. Res.* 16:272–279.
14. Lindskog, S. 1982. carbonic anhydrase. *Adv. Inorg. Biochem.* 4:115–170.
15. Emerson, S. D., and G. N. La Mar. 1990. NMR determination of the orientation of the magnetic susceptibility tensor in cyanometmyoglobin: a new probe of steric tilt of bound ligand. *Biochemistry.* 29:1556–1566.
16. Yamamoto, Y., N. Nanai, and R. Chujo. 1990. Mapping paramagnetic metal-centered dipolar field in haemoprotein using haem methyl carbon and the attached proton resonance. *J. Chem. Soc. Chem. Commun.* 22:1556–1557.
17. Bertini, I., A. Dei, C. Luchinat, and R. Monnanni. 1985. Acid-base properties of cobalt(II)-substituted carbonic anhydrases. *Inorg. Chem.* 24:301–303.
18. Banci, L., I. Bertini, C. Luchinat, R. Monnanni, and J. M. Moratal Mascarell. 1989. ^{1}H NMR spectra of cobalt(II)-substituted carbonic anhydrase isoenzymes. *Gazz. Chim. Ital.* 119:23–29.
19. Bertini, I., C. Luchinat, and A. Scozzafava. 1982. Carbonic anhydrase: an insight into the zinc binding site and into the active cavity through metal substitution. *Struct. Bonding.* 48:45–92.
20. Banci, L., I. Bertini, C. Luchinat, A. Donaire, M.-J. Martinez, and J. M. Moratal Mascarell. 1990. The factors governing the coordination number in the anion derivatives of carbonic anhydrase. *Comments Inorg. Chem.* 9:245–261.
21. Eriksson, A. E., P. M. Kylsten, T. A. Jones, and A. Liljas. 1989. Crystallographic studies of inhibitor binding sites in carbonic anhydrase II: A pentacoordinated binding of the NCS^- ion to the zinc at high pH. *Proteins.* 4:283–293.
22. Hunt, J. B., M. J. Rhee, and C. B. Storm. 1977. A rapid and convenient preparation of Apocarbonic Anhydrase. *Anal. Biochem.* 55:614–617.
23. Inubushi, T., and E. D. Becker. 1983. Efficient detection of paramagnetically shifted NMR resonances by optimizing the WEFT pulse sequence. *J. Magn. Reson.* 51:128–133.
24. Vold, R. L., J. S. Waugh, M. P. Klein, and D. E. Phelps. 1968. Measurement of spin relaxation in complex systems. *J. Chem. Phys.* 48:3831–3832.
25. Markley, J. L., W. J. Horsley, and M. P. Klein. 1971. Spin-lattice relaxation measurements in slowly relaxing complex spectra. *J. Chem. Phys.* 55:3604–3605.
26. Banci, L., I. Bertini, C. Luchinat, M. Piccioli, A. Scozzafava, and P. Turano. 1989. ^{1}H NOE studies on Dicopper(II) Dicobalt(II) Superoxide Dismutase. *Inorg. Chem.* 28:4650–4656.
27. Redfield, A. G., S. D. Kunz, and E. K. Ralph. 1975. Dynamic range in Fourier transform proton magnetic resonance. *J. Magn. Reson.* 19:114–117.
28. Johnson, R. D., S. Ramaprasad, and G. N. La Mar. 1983. A method of assigning functionally relevant amino acid residue resonances in paramagnetic hemoproteins using proton NOE measurements. *J. Am. Chem. Soc.* 105:7205–7206.
29. Ramaprasad, S., R. D. Johnson, and G. N. La Mar. 1984. Vinyl mobility in myoglobin as studied by time-dependent nuclear Overhauser effect measurements. *J. Am. Chem. Soc.* 106:3632–3635.

30. Banci, L., I. Bertini, C. Luchinat, and M. Piccioli. 1990. Transient versus steady state NOE in Paramagnetic molecules Cu_2Co_2SOD as an example. *FEBS (Fed. Eur. Biochem. Soc.) Lett.* 272:175–180.

31. Banci, L., I. Bertini, C. Luchinat, and M. Piccioli. 1991. Frontiers in NMR of paramagnetic molecules: ^1H NOE and related experiments. *In* NMR and biomolecular structure. N. Niccolai, editor. VCH Publishers, Weinteim, Germany. 31–60.

32. Macura, S., K. Wüthrich, and R. R. Ernst. 1982. The relevance of J cross-peaks in two-dimensional NOE experiments of macromolecules. *J. Magn. Reson.* 47:351–357.

33. Marion, D., and K. Wüthrich. 1982. Application of phase sensitive 2-dimensional correlated spectroscopy (COSY) for measurements of ^1H–^1H spin–spin constants in proteins. *Biochem. Biophys. Res. Commun.* 113:967–974.

34. Aue, W. P., E. Bartholdi, and R. R. Ernst. 1976. Two dimensional spectroscopy. Application to nuclear magnetic resonance. *J. Chem. Phys.* 64:2225–2246.

35. Wüthrich, K. 1986. NMR of protein and nucleic acids. John Wiley and Sons, Inc. New York.

36. Gros, K. H., and H. R. Kalbitzer. 1988. Distribution of chemical shifts in ^1H nuclear magnetic resonance spectra of proteins. *J. Magn. Reson.* 76:87–99.

37. Kannan, K. K., K. Nostrand, S. Fridborg, A. Lovgren, A. Ohlsson, and M. Petef. 1975. Crystal structure of human erythrocyte carbonic anhydrase B. Three-dimensional structure at a nominal 2.2-Å resolution. *Proc. Natl. Acad. Sci. USA.* 72:51–55.

38. Andersson, B., P. O. Nyman, and L. B. Strid. 1972. Amino acid sequence of human erythrocyte carbonic anhydrase B. *Biochem. Biophys. Res. Commun.* 48:670–6770.

39. Tashian, R. E. 1989. The carbonic anhydrase: widening perspectives of their evolution, expression and function. *Bioessays.* 10:186–192.

41. Bertini, I., G. Canti, C. Luchinat, and F. Mani. 1981. ^1H NMR spectra of the coordination sphere of cobalt-substituted Carbonic Anhydrase. *J. Am. Chem. Soc.* 103:7784–7788.